Current Science
CS 5 (5), 4974-4996 (2025)
Received 11 July 2025 | **Revised 17 August** 2025 | **Accepted 19 September** 2025 | **Online Available 22 October** 2025
https://doi.org0/10.52845/CS/2025-5-5-49

Current Science
Current Science

OPEN ACCESS
ISSN(O)2795-8639

Original Article

Research on Sliding Mode Robust Synchronous Control Strategy for the Lifting Hydraulic System of a Subsea Drilling Rig Frame

Lieyu Tian[1], Kang Lin[1,*], Xianglin Qu[2,3], Huiyin Zhang[1], Xinyu Zhao[2], Junguo Cui[2], Wensheng Xiao [2]

[1]Guangzhou Marine Geological Survey, China Geological Survey, Guangzhou 511458, China

[2]College of Mechanical and Electrical Engineering, China University of Petroleum, Qingdao 266580, China

[3]Yantai CIMC Raffles Offshore Ltd, Yantai, 264670, PR China

[*]Corresponding Author: Kang Lin

Abstract:
Addressing the challenge of insufficient synchronization accuracy in the four hydraulic cylinders during the lifting and lowering operations of a subsea drilling rig frame, this paper proposes a multi-cylinder synchronous control strategy. This strategy integrates an improved cross-coupling synchronization error, an adaptive parameter law, and sliding mode robust control. A nonlinear dynamic model of the four-cylinder lifting system is established to analyze the interaction mechanism between the coupling forces and displacement errors among the hydraulic cylinders under unbalanced and varying load conditions. On this basis, a sliding mode controller is designed utilizing the cross-coupling error. An adaptive algorithm is introduced to update system parameters online, and a saturation function is employed to suppress sliding mode chattering, thereby enhancing system robustness and synchronization precision. Co-simulations via AMESim and MATLAB/Simulink, along with experimental validation, demonstrate that the proposed control strategy achieves high-precision synchronous motion of the four hydraulic cylinders in both lifting and lowering scenarios. The maximum tracking error is confined to 1.67 mm, and the steady-state error is maintained within 0.48 mm. The strategy effectively mitigates the impact of time-varying loads and external disturbances, significantly improving the stability and reliability of the subsea drilling rig frame during lifting and lowering operations.

Keywords: Elevator frame; Hydraulic system; Synchronization control

Introduction

Natural gas hydrate is widely recognized as an efficient and clean alternative energy source to conventional oil and natural gas. Trial production typically employs depressurization methods conducted from floating drilling platforms, as shown in Figure 1 [1]. However, this approach involves high costs associated with the construction of drilling platforms and extraction operations, making economical exploitation unfeasible.

The subsea drilling rig represents a groundbreaking innovative concept in offshore oil and gas equipment. It involves installing a newly designed, streamlined deepwater drilling system directly on the seabed mudline and incorporates an innovatively designed dual-base structure for the rig frame. A new drilling and production process, driven directly by permanent magnet motors, is adopted. Only a single umbilical cable is required to connect the subsea drilling rig to the

support vessel, enabling remote control and power transmission. This system offers advantages such as lower drilling costs, high efficiency, enhanced safety, easier pressure maintenance, compact equipment size, ease of operation, and strong adaptability to various vessels.

(a) (b)

Figure 1 Picture of first NGH production test in the SCS. The production test platform 'BLUEWHALE #1' (a) and the flame from the venting *gas (b).*

The frame is divided into an upper module and a lower module. The lifting and lowering between these two modules is actuated by four hydraulic cylinders. Core equipment is mounted on the upper module, while the hydraulic power unit and auxiliary tools are installed on the lower module. During initial deployment or when the tool string requires replacement, the upper and lower modules are extended, positioning the rig at its maximum height to ensure the entire tool string can be fully accommodated within the system. During normal drilling operations, the modules are retracted, lowering the rig to enhance the overall structural stability during drilling. Schematic diagrams illustrating the raised and lowered states of the subsea drilling rig frame are shown in Figure 2.

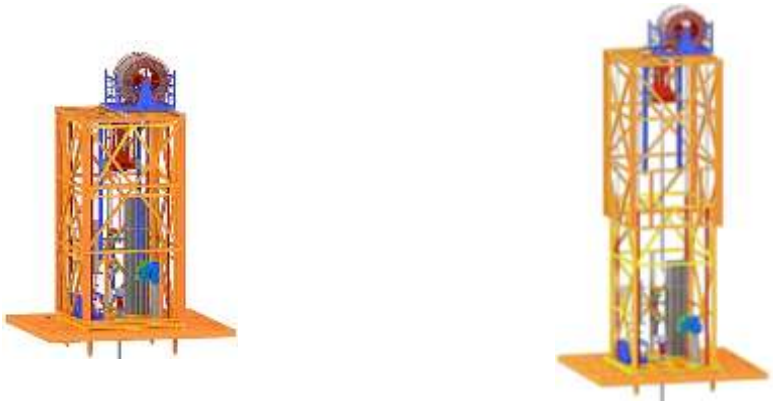

(a) Schematic of the frame in lowered position *(b) Schematic of the frame in raised position*

Figure 2 Schematic diagram of the lifting system for the underwater drilling rig frame

In the design of a variable-height frame, the synchronous lifting and lowering of the upper module by the four hydraulic cylinders is essential. The precision of this synchronized displacement is critical. If the displacement of the hydraulic cylinders is not synchronized or exhibits significant error, it may lead to tilting of the upper platform, instability of core equipment, and other chain reactions. Excessive displacement error may even cause accidents such as

overturning or fracture of the upper platform. Therefore, research on the synchronization control performance of the lifting hydraulic system for the subsea drilling rig frame is of great importance.

Classical linear control theory, developed in the mid-20th century, is built upon the fundamental assumption that system dynamics can be linearly decomposed. By establishing a transfer function framework and employing frequency-domain analysis tools, it ensures system stability 1. Among these, the most representative control strategy is the PID control algorithm 3.However, for the four-cylinder lifting hydraulic system of the subsea drilling rig frame studied in this paper, the response speed and control accuracy of PID control fall far short of the design requirements. Therefore, more complex and advanced control algorithms must be introduced.

Nonlinear control theory has achieved breakthrough progress in recent years 4. Its core lies in constructing a model-driven theoretical framework and systematically addressing inherent challenges in electro-hydraulic servo systems—such as parameter perturbations, nonlinear coupling, and unknown disturbances—through methods like backstepping design 5, adaptive algorithms 6, robust algorithms 7, and observer construction 8.

Sliding mode control (SMC) has become an effective method for addressing complex disturbances in hydraulic systems due to its fast response characteristics for complex nonlinear systems. Its control principle involves constructing a sliding surface and using a controller with switching terms to force the system trajectory to converge along the desired trajectory. In the presence of system modeling uncertainties and external disturbances, the strong robustness of sliding mode control ensures that system errors converge to a bounded region within finite time and achieve asymptotic stability. Du et al. proposed a sliding mode control algorithm based on a state observer, significantly enhancing system robustness 9. Xu et al. introduced an integral sliding mode coupling control algorithm that incorporates nonlinear differential control to suppress chattering, greatly improving control accuracy 10. Qiang et al. achieved stable control of hydraulic execution units under complex disturbances using an algorithm combining RBF radial basis function and sliding mode control 11. Current methods for suppressing chattering mainly include introducing higher-order sliding modes 12, designing saturation functions 13, and constructing reaching laws. Tran et al. proposed a sliding mode control algorithm based on a high-gain observer, effectively suppressing chattering 14. Additionally, sliding mode control must consider whether the actual system can achieve the desired control capability 15, meaning verification is necessary after controller design 16 - 17. Liu et al. used a differential evolution algorithm and linear matrix inequality-based H^{∞} optimization method to ensure system constraint requirements 18.

Multi-cylinder synchronous control systems offer significant advantages in terms of power density, dynamic response, and control accuracy. Existing research primarily focuses on three aspects: displacement synchronization, force synchronization, and velocity synchronization. However, due to nonlinear disturbances, parameter uncertainties, and coupled external interferences, achieving ideal consistency control among actuating units remains challenging. Within classical control architectures, master-slave control, parallel control, and cross-coupling control form the three fundamental theoretical frameworks 19.

(1) Master-Slave Synchronous Control Strategy

The core of the master-slave synchronization control architecture lies in establishing a hierarchical tracking system. In this strategy, the

master hydraulic cylinder tracks the desired trajectory via closed-loop control and transmits its real-time displacement signal as a dynamic reference input to the other cylinders, thereby achieving coordinated following motion among multiple actuators. This method is particularly suitable for systems where hydraulic cylinders exhibit significant differences in dynamic response. By designating the cylinder with slower response as the master, faster-response units are compelled to perform dynamic compensation.

However, a inherent limitation of this approach is error accumulation. When the dynamic characteristics between the master and slave units differ considerably, synchronization phase error may increase quadratically, severely limiting the system's disturbance rejection capability. The research team of Zhang 20 further incorporated fuzzy control theory, using triangular membership functions to dynamically adjust control gains, which significantly improved the steady-state accuracy of trajectory tracking. These results demonstrate that integrating intelligent control algorithms into the master-slave framework can effectively enhance the precision of classical control theories.

(2) Parallel Synchronous Control Strategy

Parallel synchronous control employs independent closed-loop architecture, where each hydraulic cylinder performs decoupled control based on the same desired trajectory. Since there is no dynamic coupling between the loops, this strategy offers local disturbance isolation. It demonstrates satisfactory synchronization performance under ideal disturbance-free conditions; however, disturbances are inevitable in practical engineering applications, necessitating highly robust single-cylinder controllers. The advantages of this method include notable structural decoupling characteristics and ease of parameter tuning. Nevertheless, due to the lack of a cooperative compensation mechanism, synchronization accuracy is limited, making it suitable for industrial applications where high precision is not critical. To overcome these limitations, Zhang's team 21 implemented a fuzzy PID algorithm in a dual-cylinder system, using membership functions to adjust gain parameters online. Experimental results showed that the synchronization error could be stabilized within a small threshold.

(3) Cross-Coupling Synchronous Control Strategy

Cross-coupling control utilizes a real-time synchronization error compensation mechanism, where weighted phase differences are fed back to individual hydraulic cylinders, forming a multi-cylinder cooperative compensation network 22. This strategy exhibits high synchronization accuracy and strong disturbance rejection in dual-cylinder systems. However, its extension to multi-cylinder systems encounters the "curse of dimensionality": the dimension of the coupling gain matrix grows exponentially for systems with three or more axes, necessitating dimensionality reduction techniques such as deviation coupling or ring topology simplification. For complex applications, Yang 23 designed a pre-compensation decoupling algorithm that suppresses dynamic coupling effects among hydraulic robotic joints through a feedforward channel, greatly enhancing the trajectory tracking accuracy of a six-degree-of-freedom platform.

To address core challenges such as time-varying loads, parameter uncertainties, and uneven dynamic coupling in multi-cylinder systems, this paper proposes an integrated multi-cylinder synchronous control strategy. This approach combines an improved cross-coupling synchronization error mechanism, an adaptive parameter law, and sliding mode robust control.

2. Modeling of the Four-Cylinder Lifting System for the Subsea Drilling Rig Frame

2.1 Flow Equation for the Proportional Servo Valve of the Hydraulic Cylinder

The three-position four-way proportional servo valve serves as the core control unit in the lifting hydraulic system of the subsea drilling rig frame. Therefore, this section establishes the flow equation for the proportional servo valve of the hydraulic cylinder.

With the extension direction of the piston rod defined as positive, the flow rates controlled by the proportional servo valve into the two chambers during piston rod extension are calculated as follows:

$$\begin{cases} Q_1 = C_d \omega x_v \sqrt{\frac{2}{\rho}(P_s - P_1)} \\ Q_2 = C_d \omega x_v \sqrt{\frac{2}{\rho}(P_2 - P_r)} \end{cases} \tag{1}$$

Similarly, when the hydraulic cylinder moves in the reverse direction, the flow rates controlled by the proportional servo valve into the two chambers are calculated as follows:

$$\begin{cases} Q_1 = C_d \omega x_v \sqrt{\frac{2}{\rho}(P_1 - P_r)} \\ Q_2 = C_d \omega x_v \sqrt{\frac{2}{\rho}(P_s - P_2)} \end{cases} \tag{2}$$

The flow gain coefficient k_q of the proportional servo valve is defined as:

$$k_q = C_d \omega \sqrt{\frac{2}{\rho}} \tag{3}$$

By combining Eq. (1) to Eq. (3), the flow rates controlled by the proportional servo valve into the two chambers of the hydraulic cylinder can be comprehensively expressed as:

$$\begin{cases} Q_1 = k_q x_v \left[s(x_v)\sqrt{P_s - P_1} + s(-x_v)\sqrt{P_1 - P_r} \right] \\ Q_2 = k_q x_v \left[s(x_v)\sqrt{P_2 - P_r} + s(-x_v)\sqrt{P_s - P_2} \right] \end{cases} \tag{4}$$

where, $s(*)$ denotes a semi-sign function, defined as follows:

$$s(*) = \begin{cases} 1, if * \geq 0 \\ 0, if * < 0 \end{cases} \tag{5}$$

Due to the relatively low operating speed of the lifting hydraulic system in the subsea drilling rig frame, the response speed of the proportional servo valve is sufficiently fast. Therefore, the spool displacement x_v of the proportional servo valve can be linearly related to the control input u s follows:

$$x_v = k_v u \tag{6}$$

were, k_v is the voltage-spool displacement gain coefficient of the proportional servo valve.

Finally, the flow rates into the rod chamber and rodless chamber of the lifting hydraulic cylinder can be expressed in terms of the control input by Eq. (7):

$$\begin{cases} Q_1 = k_t u\left[s(x_v)\sqrt{P_s - P_1} + s(-x_v)\sqrt{P_1 - P_r}\right] \\ Q_2 = k_t u\left[s(x_v)\sqrt{P_2 - P_r} + s(-x_v)\sqrt{P_s - P_2}\right] \end{cases} \tag{7}$$

Where, $k_t = k_q \cdot k_v$ is the total gain coefficient relative to the control input.

2.2 Flow Continuity Equation for the Hydraulic Cylinder

Based on the flow rate equations for the rod and rodless chambers of the hydraulic cylinder given in Eq. (7), the flow continuity equation for the lifting hydraulic cylinder can be further established. Taking into account the oil compressibility during the operation of the lifting hydraulic system, the pressure-flow dynamics for the two chambers are expressed as:

$$\begin{cases} \dot{P}_1 = \dfrac{\beta_e}{V_1}\left[Q_1 - A_1\dot{y} - C_t(P_1 - P_2)\right] + \Delta_1 \\ \dot{P}_2 = \dfrac{\beta_e}{V_1}\left[-Q_2 + A_2\dot{y} + C_t(P_1 - P_2)\right] + \Delta_2 \end{cases} \tag{8}$$

The state variable representing the actual displacement of the hydraulic cylinder piston rod is defined as:

$$x = [x_1, x_2, x_3]^T \tag{9}$$

Where, $x \in \mathbb{R}^3$ denotes the state vector comprising the actual displacement, actual velocity, and actual acceleration of the piston rod.

Finally, by integrating the aforementioned load dynamics equation, flow dynamic equation, and state variables, the state-space equation of the lifting hydraulic system for the subsea drilling rig frame can be derived as follows:

$$\begin{cases} \dot{x}_1 = x_2 \\ \dot{x}_2 = x_3 \\ \dot{x}_3 = -g_0 x_2 - Bx_3 - \varphi\Delta P + gu + d(t) \end{cases} \tag{10}$$

Where,g is the control gain of the hydraulic system; $d(t)$ represents the lumped uncertainty caused by external disturbances and inherent nonlinearities of the hydraulic system.

3. Theoretical Design of a Sliding Mode Robust Synchronous Control Strategy for the Subsea Drilling Rig Frame Lifting Hydraulic System

Due to the varying coupling forces among the four hydraulic cylinders, the input and output characteristics of each cylinder differ. It is necessary to introduce a multi-cylinder displacement coupling error and a synchronous controller to achieve overall coordination between the cylinders.

3.1 Control System Modeling

As established in Chapter 2, a nonlinear model of the single-cylinder valve-controlled lifting

hydraulic system of the subsea drilling rig frame was developed. The design of the sliding mode robust synchronous controller, based on cross-coupling synchronization error and an adaptive algorithm, builds upon the state equation shown in Eq. (10) after it passes through a transformation.

The mathematical model of the four-cylinder synchronous lifting system can be expressed as:

$$\begin{cases} \dot{x}_1 = x_2,\ \dot{x}_2 = x_3,\ \dot{x}_3 = -g_0 x_2 - Bx_3 - \varphi \Delta P + gv(t) + g\Phi_r + d(t) \\ x_1 = [x_{11}, x_{12}, x_{13}, x_{14}],\ x_2 = [x_{21}, x_{22}, x_{23}, x_{24}],\ x_3 = [x_{31}, x_{32}, x_{33}, x_{34}] \\ g_0 = \mathrm{diag}\{g_{01}, g_{02}, g_{03}, g_{04}\},\ g = \mathrm{diag}\{g_1, g_2, g_3, g_4\} \\ B = \mathrm{diag}\{B_1, B_2, B_3, B_4\},\ B_i = \dfrac{b_i}{m_i} \\ u = [u_1, u_2, u_3, u_4]^T,\ \varphi = \mathrm{diag}\{\varphi_1, \varphi_2, \varphi_3, \varphi_4\} \\ \Delta P = [\Delta P_1, \Delta P_2, \Delta P_3, \Delta P_4],\ d(t) = [d_1(t), d_2(t), d_3(t), d_4(t)]^T \end{cases} \tag{11}$$

The remaining parameters are defined as follows:

$$\begin{aligned} & g_{0i} = \frac{\beta_{ei}}{m_i}\left(\frac{A_1^2}{V_1} + \frac{A_2^2}{V_2}\right),\ \varphi_i = \frac{\beta_{ei} C_{ti}}{m_i}\left(\frac{A_1}{V_1} + \frac{A_2}{V_2}\right), \\ & \Delta P_i = P_{1i} - P_{2i},\ g_i = \frac{k_t \beta_{ei}}{m_i}\left(\frac{A_1 R_{1i}}{V_1} + \frac{A_2 R_{2i}}{V_2}\right) \neq 0, \\ & R_{1i} = s(u_i)\sqrt{P_s - P_{1i}} + s(-u_i)\sqrt{P_{1i} - P_r}, \\ & R_{2i} = s(u_i)\sqrt{P_{2i} - P_r} + s(-u_i)\sqrt{P_s - P_{2i}}, \\ & d_i(t) = -\frac{\dot{F}_d + \dot{f}_c}{m} + \frac{A_1 \Delta_1 - A_2 \Delta_2}{m} \end{aligned} \tag{12}$$

Introducing adaptive parameters, the uncertain parameter vector of the system is defined as:

$$\begin{aligned} \theta &= [\theta_{11}, \theta_{12}, \theta_{13}, \theta_{14}, \theta_{21}, \theta_{22}, \theta_{23}, \theta_{24}, \theta_{31}, \theta_{32}, \theta_{33}, \theta_{34}, \theta_{41}, \theta_{42}, \theta_{43}, \theta_{44}]^T \\ &= [g_{01}, B_1, \varphi_1, g_1, g_{02}, B_2, \varphi_2, g_2, g_{03}, B_3, \varphi_3, g_3, g_{04}, B_4, \varphi_4, g_4]^T \end{aligned} \tag{13}$$

Eq.(11) can be rewritten as:

$$\begin{cases} \dot{x}_1 = x_2,\ \dot{x}_2 = x_3 \\ \dot{x}_3 = \phi(t)\theta + d(t) \end{cases} \tag{14}$$

where $\boldsymbol{\phi}^T(\boldsymbol{t})$ is the variable matrix defined as:

$$\phi^T(t) = \begin{bmatrix} -x_{21}, -x_{31}, -\Delta P_1, v_1\Phi_r, 0, 0, 0, 0, 0, 0, 0, 0, 0, 0, 0, 0 \\ 0, 0, 0, 0, -x_{22}, -x_{32}, -\Delta P_2, v_2\Phi_r, 0, 0, 0, 0, 0, 0, 0, 0 \\ 0, 0, 0, 0, 0, 0, 0, 0, -x_{23}, -x_{33}, -\Delta P_3, v_3\Phi_r, 0, 0, 0, 0 \\ 0, 0, 0, 0, 0, 0, 0, 0, 0, 0, 0, 0, -x_{24}, -x_{34}, -\Delta P_4, v_4 + \Phi_r \end{bmatrix} \tag{15}$$

Since all uncertain parameters in the system have physical meanings and their values, though variable, fall within predictable ranges, it is reasonable to assume for controller design purposes that these uncertain parameters are bounded and satisfy the following relationship:

$$\theta_1 \in \Omega_\theta \overset{def}{=} \{\theta_{1\min} \leqslant \theta_1 \leqslant \theta_{1\max}\} \tag{16}$$

The synchronous controller essentially generates the control inputs for the four servo valves. Each control input must account for the displacement errors of the other hydraulic cylinders to ensure precise synchronization of the piston displacements and accurate tracking of the desired trajectory, while also guaranteeing that the estimated system parameters remain bounded.

3.2 Design of Cross-Coupling Synchronization Error

For the four-cylinder synchronous control system, the synchronization error of the i-th cylinder is defined as:

$$z_{ei} = x_{1i} - \frac{1}{4}\sum_{j=1}^{4} x_{1j} \tag{17}$$

In the hydraulic synchronous control system, each hydraulic cylinder must not only accurately track the desired trajectory, $z_{ei} \to 0$,but also maintain consistency in displacement with the others, as expressed by Eq.(18):

$$z_{ji} = \sum_{j \neq i} k_{ij}(x_{1j} - x_{1i}) \tag{18}$$

Therefore, the cross-coupling synchronization error for the i-th cylinder in the four-cylinder synchronous control system can be defined as:

$$z_i = e_{1i} + x_{1i} - \frac{1}{4}\sum_{j=1}^{4} x_{1j} + \sum_{j \neq i} k_{ij}(x_{1j} - x_{1i}) \tag{19}$$

When $z_i \to 0$, the four-cylinder synchronous control system is guaranteed to operate smoothly and asymptotically stabilize.

By differentiating Eq. (19), the second and third derivatives of the cross-coupling error can be obtained as follows:

$$\begin{aligned}
\ddot{z}_i &= \ddot{e}_{1i} + \ddot{x}_{1i} - \frac{1}{4}\sum_{j=1}^{4} \ddot{x}_{1j} + \sum_{j \neq i} k_{ij}(\ddot{x}_{1j} - \ddot{x}_{1i}) \\
&= e_{3i} + x_{3i} - \frac{1}{4}\sum_{j=1}^{4} x_{3j} + \sum_{j \neq i} k_{ij}(x_{3j} - x_{3i}) \\
\dddot{z}_i &= \dddot{e}_{1i} + \dddot{x}_{1i} - \frac{1}{4}\sum_{j=1}^{4} \dddot{x}_{1j} + \sum_{j \neq i} k_{ij}(\dddot{x}_{1j} - \dddot{x}_{1i}) \\
&= \dot{e}_{3i} + \dot{x}_{3i} - \frac{1}{4}\sum_{j=1}^{4} \dot{x}_{3j} + \sum_{j \neq i} k_{ij}(\dot{x}_{3j} - \dot{x}_{3i})
\end{aligned} \tag{20}$$

3.3 Adaptive Parameter Design

From Section 3.1, the parameter column vector is denoted as $\theta_i = [\theta_{i1} \quad \theta_{i2} \quad \theta_{i3} \quad \theta_{i4}]^T = [g_{0i} \quad B_i \quad \varphi_i \quad g_i]^T$.

For notational convenience, let $\theta = [\theta_1 \quad \theta_2 \quad \theta_3 \quad \theta_4]^T = [g_0 \quad B \quad \varphi \quad g]^T$. The adaptive controller is designed as follows:

$$\hat{\theta}(t+1) = \hat{\theta}(t) + F(t+1)\phi(t)\epsilon(t+1) \tag{21}$$

Neglecting Φ_{ri} and $d(t)$, we obtain:

$$y(t) = -\theta_1 x_2 - \theta_2 x_3 - \theta_3 \Delta P + \theta_4 v(t) = \theta^T(t)\phi(t) \tag{22}$$

Define the a priori adjustable predictor $\hat{y}(t+1)$ as:

$$\hat{y}(t+1) = \hat{y}\left[(t+1)|\hat{\theta}(t)\right] = \hat{\theta}^T(t)\phi(t) \tag{23}$$

and define the adaptive error $\epsilon(t+1)$ as:

$$\begin{aligned} \epsilon(t+1) &= y(t+1) - \hat{y}(t+1) \\ &= y(t+1) - \hat{\theta}^T(t)\phi(t) \end{aligned} \tag{24}$$

The adaptive gain matrix is defined as:

$$F(t+1) = F(t) - \frac{F(t)\phi(t)\phi^T(t)F(t)}{1+\phi^T(t)F(t)\phi(t)} \tag{25}$$

Proof:The derivation of the above definitions is as follows. First, define the minimum cost function to quantify the error between the output of the controlled system and the output of the predictive model:

$$\min_{\hat{\theta}(t)} J(t) = \sum_{i=1}^{t}\left[y(i) - \hat{\theta}^T(t)\phi(i-1)\right]^2 \tag{26}$$

The cost function for the estimated parameter $\hat{\theta}$ is given by:

$$J(t) = \sum_{i=1}^{t}\left[y(i) - \hat{\theta}^T(t)\phi(i-1)\right]^2 \tag{27}$$

Differentiating Eq.(27) with respect to $\hat{\theta}(t)$ yields:

$$\frac{\partial J(t)}{\partial \hat{\theta}(t)} = -2\sum_{i=1}^{t}\left[y(i) - \hat{\boldsymbol{\theta}}^T(t)\phi(i-1)\right]\phi(i-1) = 0 \tag{28}$$

where,

$$\begin{aligned}\left[\hat{\theta}^T(t)\phi(i-1)\right]\phi(i-1) &= \phi(i-1)\left[\hat{\theta}^T(t)\phi(i-1)\right]^T \\ &= \phi(i-1)\phi^T(i-1)\hat{\theta}(t)\end{aligned} \tag{29}$$

Substituting Eq. (29) into Eq. (28) gives:

$$\sum_{i=1}^{t}\left[y(i)\phi(i-1) - \phi(i-1)\phi^T(i-1)\hat{\theta}(t)\right] = 0 \tag{30}$$

which is equivalent to:

$$\begin{aligned}\sum_{i=1}^{t} y(i)\phi(i-1) &= \sum_{i=1}^{t}\phi(i-1)\phi^T(i-1)\hat{\theta}(t) \\ &= \sum_{i=1}^{t}[\phi(i-1)\phi^T(i-1)]\hat{\theta}(t)\end{aligned} \tag{31}$$

From this, the estimated parameter $\hat{\theta}(t)$ at the current time t can be obtained as:

$$\hat{\theta}(t) = \left[\sum_{i=1}^{t}\phi(i-1)\phi^T(i-1)\right]^{-1}\sum_{i=1}^{t} y(i)\phi(i-1) = F(t)\sum_{i=1}^{t} y(i)\phi(i-1) \tag{32}$$

The adaptive gain matrix $F(t)$ is defined as:

$$F(t) = \left[\sum_{i=1}^{t}\phi(i-1)\phi^T(i-1)\right]^{-1} \tag{33}$$

Taking its inverse yields:

$$F^{-1}(t) = \sum_{i=1}^{t}\phi(i-1)\phi^T(i-1) \tag{34}$$

The inverse of the adaptive gain matrix at time t+1, denoted as $F^{-1}(t+1)$, is:

$$\begin{aligned}F^{-1}(t+1) &= \sum_{i=1}^{t+1}\phi(i-1)\phi^T(i-1) \\ &= F^{-1}(t) + \phi(t)\phi^T(t)\end{aligned} \tag{35}$$

Furthermore, the adaptively estimated parameter $\hat{\theta}(t+1)$ at time t+1 is:

$$\begin{aligned}\hat{\theta}(t+1) &= F(t+1)\sum_{i=1}^{t+1} y(i)\phi(i-1) \\ &= F(t+1)\left[F^{-1}(t)\hat{\theta}(t) + y(t+1)\phi(t)\right]\end{aligned} \tag{36}$$

Substituting Eq.(35) into Eq. (36) gives:

$$\begin{aligned}\hat{\theta}(t+1) &= F(t+1)\left\{\hat{\theta}(t)\left[F^{-1}(t+1) - \phi(t)\phi^T(t)\right] + y(t+1)\phi(t)\right\} \\ &= F(t+1)\left\{F^{-1}(t+1)\hat{\theta}(t) + \phi(t)\left[y(t+1) - \phi^T(t)\hat{\theta}(t)\right]\right\}\end{aligned} \tag{37}$$

Since $\phi^T(t)\hat{\theta}(t)$ is a scalar, and the transpose of a scalar equals itself, we have:

$$\phi^T(t)\hat{\theta}(t) = \left[\phi^T(t)\hat{\theta}(t)\right]^T = \hat{\theta}^T(t)\phi(t) \tag{38}$$

Substituting Eq. (24) and Eq.(38) into Eq. (37) yields Eq.(21):

$$\hat{\theta}(t+1) = \hat{\theta}(t) + F(t+1)\phi(t)\epsilon(t+1) \quad (39)$$

This completes the proof of the indirect adaptive parameter estimation for $\hat{\theta}(t+1)$.

Lemma 1: If F and R are non-singular matrices, and H is a full-rank matrix, then the following equality holds:

$$(F^{-1} + HR^{-1}H^T)^{-1} = F - FH(R + H^T FH)^{-1}H^T F \quad (40)$$

Applying Lemma 1, Eq. (35) can be rewritten as:

$$\begin{aligned} F(t+1) &= [F^{-1}(t) + \phi(t)\phi^T(t)]^{-1} \\ &= F(t) - \frac{F(t)\phi(t)\phi^T(t)F(t)}{1+\phi^T(t)F(t)\phi(t)} \end{aligned} \quad (41)$$

With this formula, updating from $F(t)$ to $F(t+1)$ requires only quantities at time t, without the need for historical data. The denominator $1+\phi^T(t)F(t)\phi(t)$ is also a scalar.

This concludes the proof of the iterative indirect adaptive parameter update procedure. The key equations are summarized in Eq. (21) to Eq. (25).

3.4 Design of the Four-Cylinder Synchronous Controller

Sliding mode variable structure control is a typical nonlinear robust control strategy, whose essence lies in achieving strong convergence of system trajectories through switching actions. This method helps overcome parameter uncertainties and time-varying disturbances, making it suitable for suppressing cross-coupling synchronization errors. However, traditional sliding mode control suffers from chattering caused by high-frequency switching, where the system state oscillates around the sliding surface, leading to high-frequency fluctuations in the control signal. This chattering is fundamentally due to the discontinuous switching action of the sign function in the sliding mode reaching law, as illustrated in Figure 3. To address this issue, an improved sliding mode control strategy is designed to ensure high synchronization accuracy in the multi-cylinder position synchronous control system.

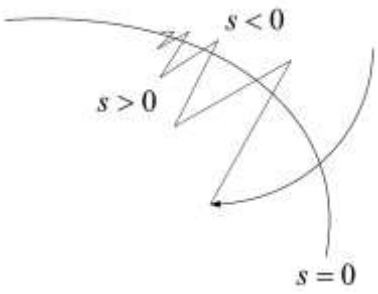

Figure3 Sliding mode chattering phenomenon

To mitigate chattering in the sliding mode control process, a quasi-sliding mode control method is employed. The saturation function is defined as:

$$\text{sat}(s) = \begin{cases} 1 & s > \phi \\ s/\phi & |s| \le \phi \\ -1 & s < -\phi \end{cases} \quad (42)$$

where, $\phi > 0$ is the boundary layer thickness, typically designed to be small, and s is the sliding surface to be designed.

Integrating the cross-coupling synchronization error with the sliding mode control method, the sliding surface is first defined $s_i = \ddot{z}_i + \lambda \dot{z}_i$. Assuming the system is on the sliding surface ($s = 0$ and $\dot{s} = 0$) and the disturbance $d(t) = 0$, the equivalent control is derived as:

$$\dot{s}_i = \dddot{z}_i + \lambda \ddot{z}_i = 0 \rightarrow -\lambda \ddot{z}_i = \dddot{z}_i \quad (43)$$

where, λ is the sliding surface gain.

$$0 \quad (44)$$

Thus, the equivalent control input of the adaptive controller based on sliding mode robust control is:

$$v_{\text{eq},i} = \frac{1}{\hat{\theta}_{4i}} \left(\frac{1}{4} \sum_{j=1}^{4} \dot{\hat{x}}_{3j} - \sum_{j \neq i} k_{ij} \left(\dot{\hat{x}}_{3j} - \dot{\hat{x}}_{3i} \right) - \lambda \ddot{z}_i - \dot{e}_{3i} + \hat{\theta}_{1i} \hat{x}_{2i} + \hat{\theta}_{2i} \hat{x}_{3i} + \hat{\theta}_{3i} \Delta P_i \right) - \Phi_r \quad (45)$$

To compensate for the disturbance $d_i(t)$, a robust term $v_{\text{rob},i}$ is added to the control law v_i:

$$v_i = v_{\text{eq},i} + v_{\text{rob},i} \quad (46)$$

The robust term must satisfy:

$$\hat{\theta}_{4i} v_{\text{rob},i} + d_i(t) = 0 \rightarrow v_{\text{rob},i} = -\frac{1}{\hat{\theta}_{4i}} d_i(t) \quad (47)$$

However, since $d_i(t)$ is unknown, it must be approximately compensated using a sign function or saturation function:

$$v_{\text{rob},i} = -\frac{k_{\text{rob},i}}{\hat{\theta}_{4i}} sat\left(\frac{s}{\phi} \right) \quad (48)$$

where, $v_{\text{rob},i}$ is the disturbance gain parameter and $v_{\text{rob},i} \geq D$, with D being the upper bound of the disturbance $d_i(t)$.

The control input of the adaptive controller based on sliding mode robust control is thus given by:

$$\begin{aligned} v_i = & \frac{1}{\hat{\theta}_{4i}} \left(\frac{1}{4} \sum_{j=1}^{4} \dot{\hat{x}}_{3j} - \sum_{j \neq i} k_{ij} \left(\dot{\hat{x}}_{3j} - \dot{\hat{x}}_{3i} \right) - \lambda \ddot{z}_i + \hat{\theta}_{1i} \hat{x}_{2i} + \hat{\theta}_{2i} \hat{x}_{3i} + \hat{\theta}_{3i} \Delta P_i \right) \\ & - \Phi_r - \frac{k_{\text{rob},i}}{\hat{\theta}_{4i}} sat\left(\frac{s}{\phi} \right) \end{aligned} \quad (49)$$

4. Simulation Analysis of the Sliding Mode Robust Synchronous Control Strategy for the Subsea Drilling Rig Frame Lifting Hydraulic System

4.1 Construction of the Control Algorithm Simulation Module

To validate the control performance of the adaptive sliding mode robust control strategy—based on the cross-coupling synchronization error—for the frame lifting hydraulic system, co-simulation was conducted using AMESim and MATLAB/Simulink. The Simulink model is shown in Figure 4, and the control strategy was compiled using S-functions in Simulink.

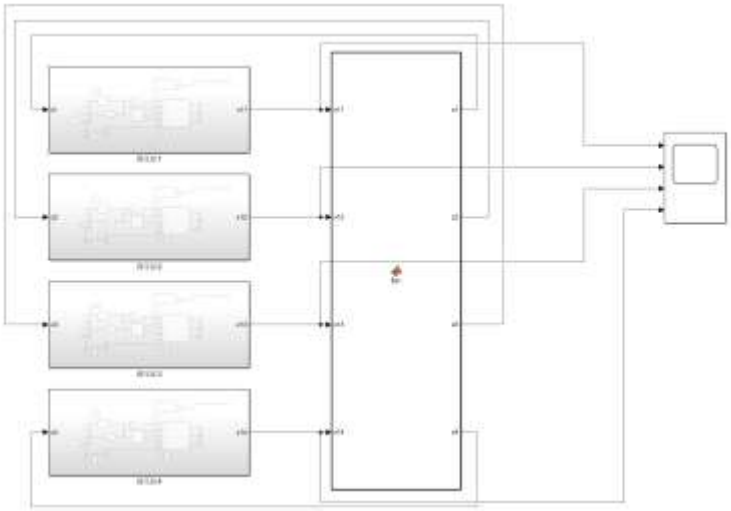

Figure 4 Simulation diagram of sliding mode robust synchronous controlsimulation diagram of adaptive robust control

An abrupt unbalanced load is defined as:

$$F_d + f_c = \begin{cases} 1.23\times10^4 v^2 & 0s \leqslant t < 300s \\ 3\times10^4 v^2 & 300s \leqslant t < 600s \\ 0.8\times10^4 v^2 & t \geqslant 900s \end{cases} \tag{50}$$

A sinusoidal function is used to represent system modeling uncertainties, yielding the disturbance $d_i(t)$ as:

$$d_i(t) = -\frac{\dot{F}_d + \dot{f}_c}{m} + d_i \sin(\pi t/100) \tag{51}$$

where, d_i, $i = 1, 2, 3, 4$ are disturbance coefficients.

4.2 Performance Analysis of the Frame Lifting Hydraulic System Under Lifting Conditions

As shown in Figures 5 and 6, a comparative analysis of the displacement tracking errors of the four hydraulic cylinders under different disturbances—controlled by the adaptive sliding mode robust algorithm based on cross-coupling synchronization error—reveals that the initial maximum error is consistently 1.67 mm. The errors converge rapidly to near zero and fluctuate within a certain steady-state range. Even when subjected to time-varying load disturbances at 300 s and 600 s, the system exhibits no significant fluctuations and quickly returns to normal operation within a short period. The overshoot percentages relative to the initial maximum error are 19%, 23%, 36%, and 27%, respectively, while the steady-state errors are 0.23 mm, 0.29 mm,

0.48 mm, and 0.35 mm, respectively.

These results demonstrate that the adaptive sliding mode robust algorithm, incorporating a sliding surface, significantly enhances the system's ability to handle abrupt disturbances from time-varying loads. The adaptive algorithm updates system parameters in real time, improving stability and disturbance rejection. Furthermore, the use of a saturation function $sat(s)$ in the quasi-sliding mode control method effectively suppresses chattering, ensuring that the tracking error is primarily influenced by internal and external disturbances. Consequently, even under internal uncertainties and harmonic fluctuations, the error remains within a small range, and the errors of the four cylinders fluctuate synchronously. This minimizes the impact of displacement discrepancies among the hydraulic cylinders, thereby greatly ensuring the stable operation of the subsea drilling rig frame lifting system.

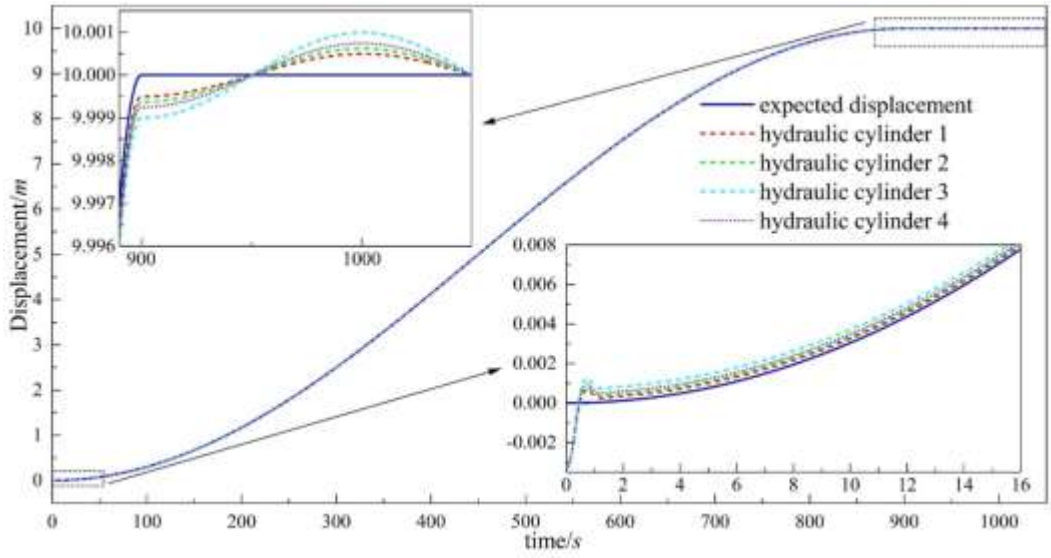

Figure 5 Comparison diagram of tracking displacement for adaptive robust control

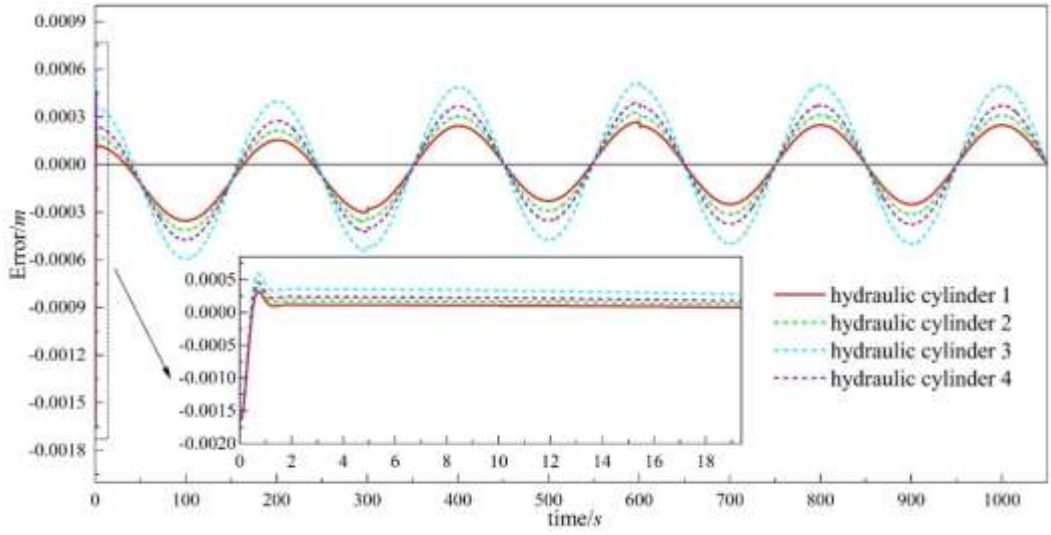

Figure 6 Comparison diagram of synchronous tracking error for adaptive sliding mode robust control

As illustrated in Figure 7, the introduction of coupling errors from the other three cylinders means that the input error is influenced not only by external disturbances but also by the displacements of the other cylinders. This allows the system to proactively compensate for phase differences among the hydraulic cylinders, preventing potential tilting or instability due to excessive displacement deviations. This enhancement in robustness significantly improves the synchronization control accuracy of the system.

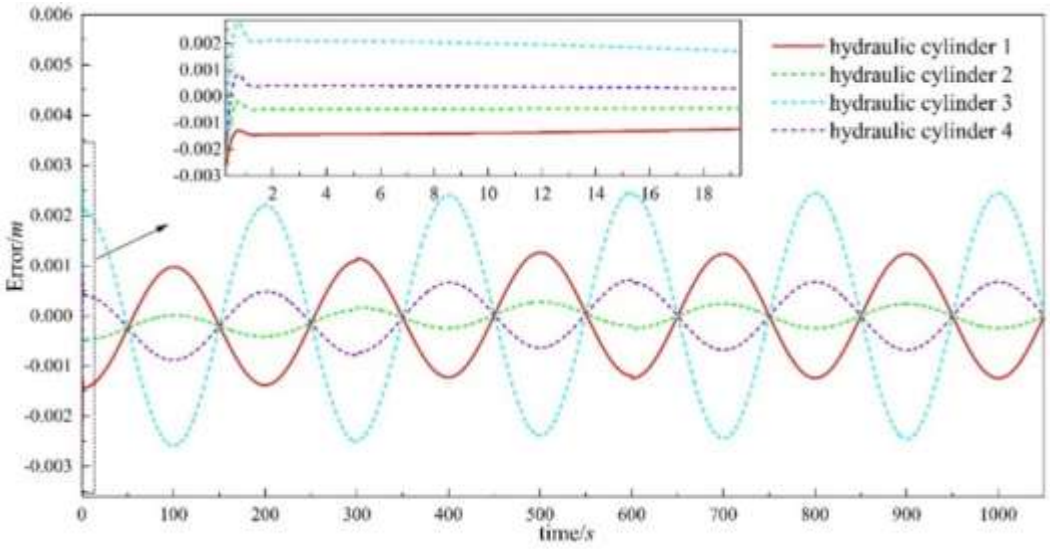

Figure 7 Comparison diagram of synchronous coupling error for adaptive sliding mode robust control

4.3 Performance Analysis of the Frame Lifting Hydraulic System Under Lowering Conditions

As shown in Figures 8 and 9, a comparative analysis of the displacement tracking errors of the four hydraulic cylinders under different disturbances during lowering operations—controlled by the adaptive sliding mode robust algorithm based on cross-coupling synchronization error—reveals that the initial maximum error is consistently 3.13 mm. The errors converge rapidly to near zero and remain within a bounded steady-state range. Despite being subjected to time-varying load disturbances at 300 s and 600 s, the system shows no significant fluctuations and recovers to normal operation quickly. The overshoot values relative to the initial maximum error are 6.70%, 11.82%, 16.93%, and 14.38%, respectively, while the steady-state errors are 0.23 mm, 0.30 mm, 0.48 mm, and 0.36 mm, respectively.

The steady-state errors are largely consistent with those observed under lifting conditions. However, the larger initial maximum error during lowering may be attributed to the increased difficulty in accurately measuring the initial position when the frame is at its highest point.

These results lead to the conclusion that the adaptive sliding mode robust algorithm based on cross-coupling synchronization error achieves high control precision, thereby greatly ensuring the stable operation of the subsea drilling rig frame lifting system.

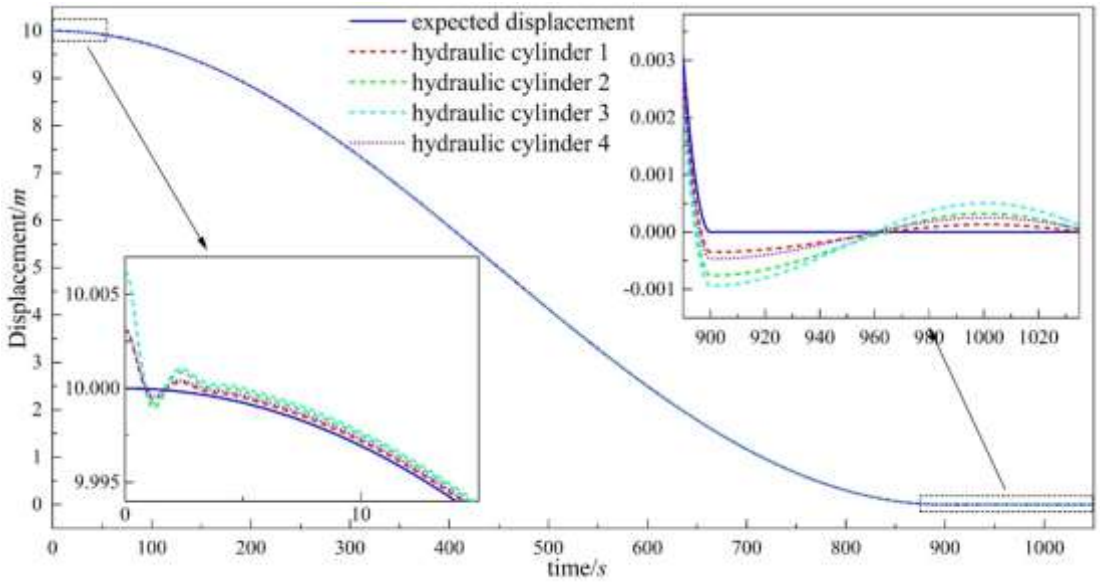

Figure8 Comparison diagram of tracking displacement for adaptive robust control

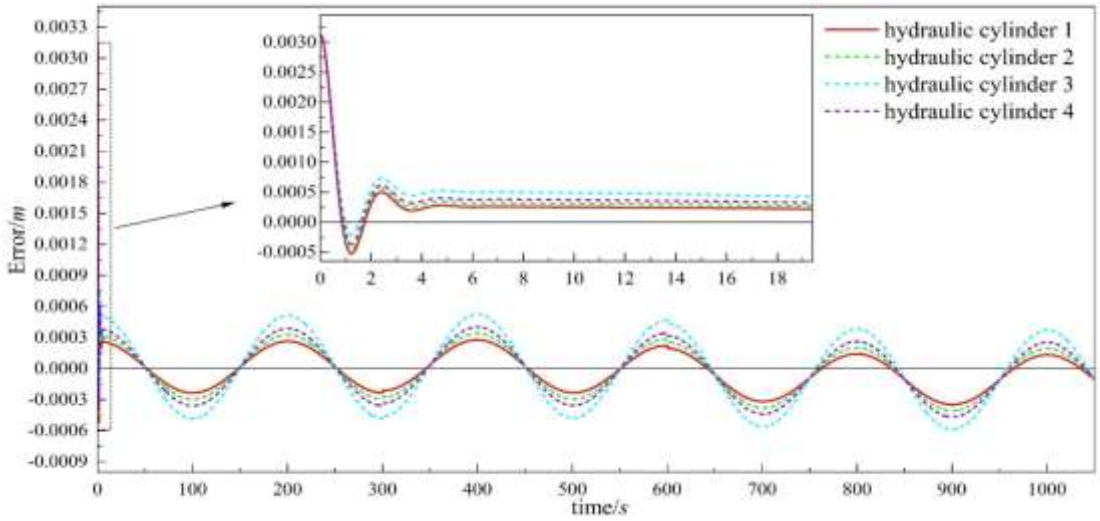

Figure 9 Comparison diagram of synchronous tracking error for adaptive sliding mode robust control

As illustrated in Figure 10, the analysis of the response curves indicates that although the initial tracking error increases, resulting in a corresponding rise in the initial coupling error, the incorporation of coupling errors from the other three cylinders allows the system input to account for not only external disturbances but also the real-time positions of the other cylinders. This enables proactive error compensation and prevents potential instability or tilting caused by excessive displacement deviations among the hydraulic cylinders.

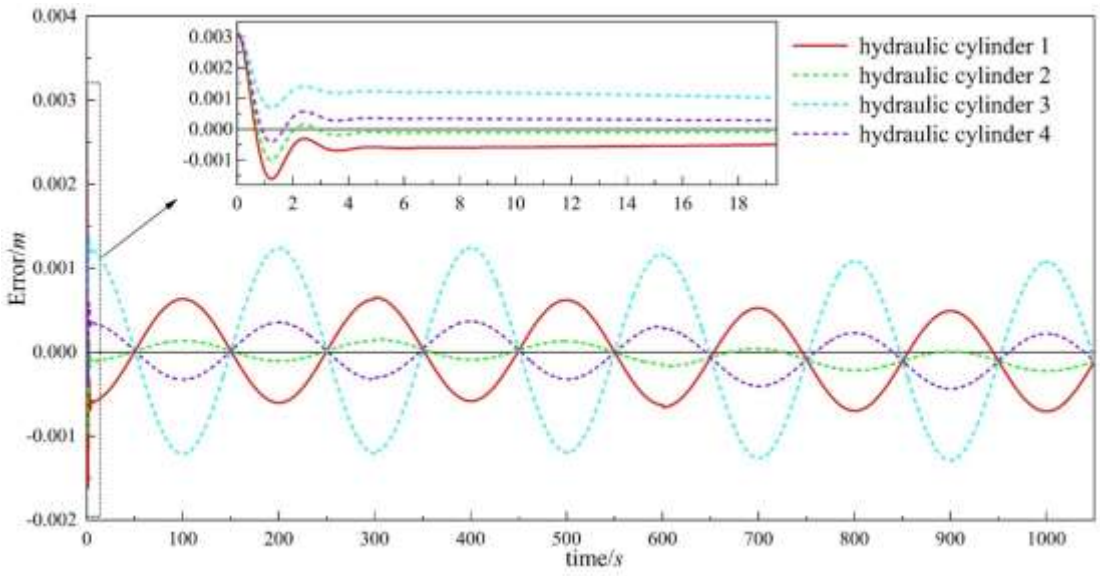

Figure 10 Comparison diagram of synchronous coupling error for adaptive sliding mode robust control

In summary, the adaptive sliding mode robust control strategy based on cross-coupling synchronization error effectively tracks the desired displacement while synchronizing inter-cylinder errors, ensuring highly stable operation of the subsea drilling rig frame lifting system under both lifting and lowering conditions.

5. Experimental Validation of the Sliding Mode Robust Synchronous Control Strategy for the Subsea Drilling Rig Frame Lifting Hydraulic System

A schematic diagram of the experimental setup for the frame lifting hydraulic system control developed in this study is shown in Figure 11. The experiment simulates the resistance during frame lifting by applying loads and unbalanced loads.

Figure11 Hydraulic system control experiment schematic diagram for frame lifting

Based on a scaled design of the frame lifting hydraulic system, the scale ratio of the test rig was determined to be 1:20. Figure 12 shows the experimental model of the frame lifting system. The upper frame model has a total height of 700 mm, a width of 610 mm, and a height of 610 mm; the lower frame model has a total height of 600 mm, a width of 660 mm, and a height of 600 mm. The frame models are made of carbon structural steel.

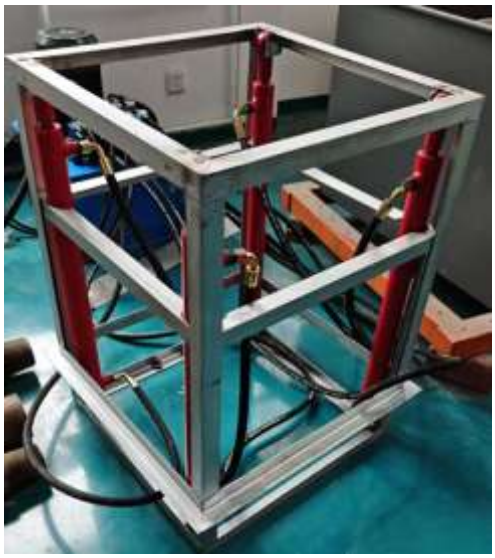

Figure 12 Schematic diagram of frame lifting experiment and hydraulic system

Figure 13 illustrates the real-time measurement and control system of the experimental platform for the subsea drilling rig frame lifting hydraulic system. The hardware of the measurement and control system mainly consists of an upper computer (PC), a lower computer (industrial PC), and a PCI-6229 data acquisition card. The specifications and models of the main components are listed in Table 1.

Figure 13 Host computer and slave computer

Table 1 Specifications and models of main components

Name	Model	Quantity
Displacement Sensor	CI43-6-1 BR01T103	4
Data Acquisition Card	PCI-6229	1
Host Computer	Vostro 3460	1
Industrial PC/PLC	4U	1

The synchronous control algorithm for the frame lifting hydraulic system was first compiled in MATLAB, and then the code was downloaded to the lower computer. Communication between the upper and lower computers was established via the TCP/IP protocol. During the experiment, sensors collected system state signals during motion and transmitted analog signals to the data acquisition card, which converted them into digital signals and sent them to the industrial PC. Simultaneously, the digital signals output by the industrial PC were converted into analog signals

to control the proportional servo valve for lifting and lowering actions.

Experimental analysis and validation were conducted on the sliding mode robust control algorithm incorporating cross-coupling error and adaptive mechanisms. The experiment involved lifting the upper frame and a load weighing 500 kg to a height of 0.5 m. The desired lifting trajectory is given by:

$$y_{1d}=\begin{cases}-0.25\cos(\pi t/45)+0.25, t<45s\\ 0.5, t\geq 45s\end{cases}$$
$$y_{2d}=\begin{cases}0.25\cos(\pi t/45)+0.25, t<45s\\ 0.5, t\geq 45s\end{cases} \quad (52)$$

Considering the abrupt unbalanced load used to define external disturbances, $d(t)$ is obtained as:

$$d(t)=\begin{cases}1000+d_iN\ \ 0s\leq t<15s\\ 5000+d_iN\ \ 15s\leq t<30s\\ 500+d_iN\ \ \ t\geq 30s\end{cases} \quad (53)$$
$$d_1=500,\ d_2=250\sqrt{2},\ d_3=0,\ d_4=250\sqrt{2}$$

The tracking errors of the four hydraulic cylinders are shown in Figures 14 to 17. The experimental disturbances and parameters were incorporated into a co-simulation in MATLAB/AMESim, yielding simulated displacement errors for the four hydraulic cylinders under experimental conditions. A comparison reveals that the experimental data closely match the simulation results. Detailed experimental data are provided in Table 2.

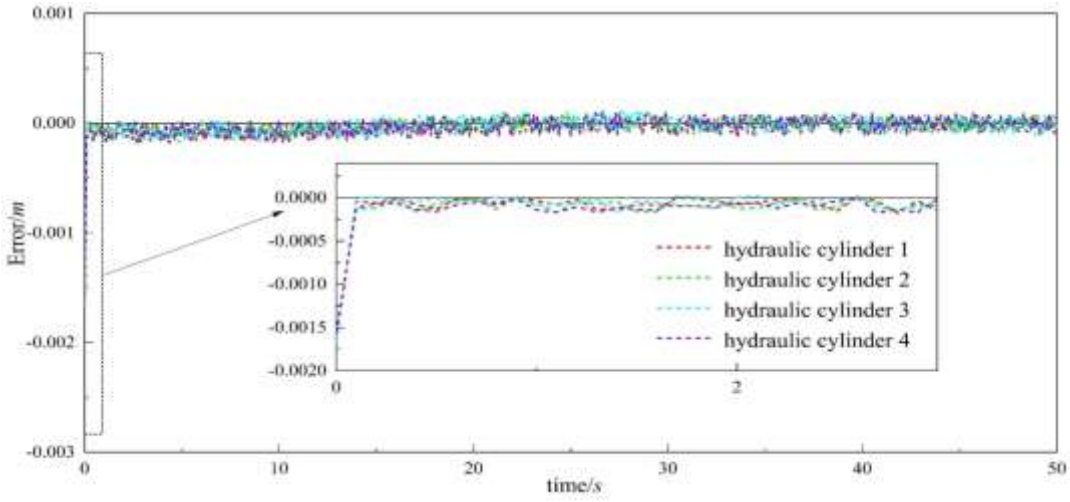

Figure 14 Comparison diagram of synchronous tracking error for adaptive sliding mode robust control

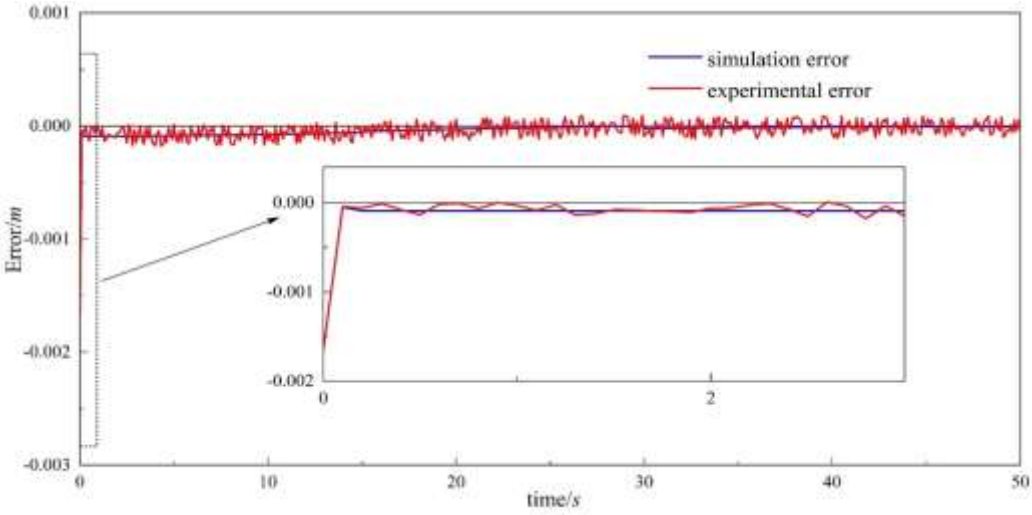

Figure15 Comparison of Synchronization Errors between Experimental and Simulation Results for Hydraulic Cylinder 1

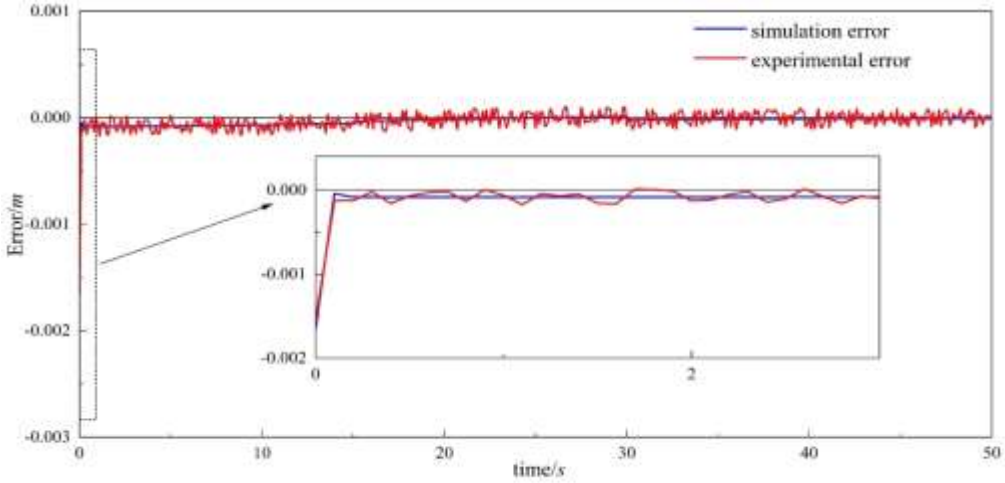

Figure 16 Comparison of Synchronization Errors between Experimental and Simulation Results for Hydraulic Cylinder 2

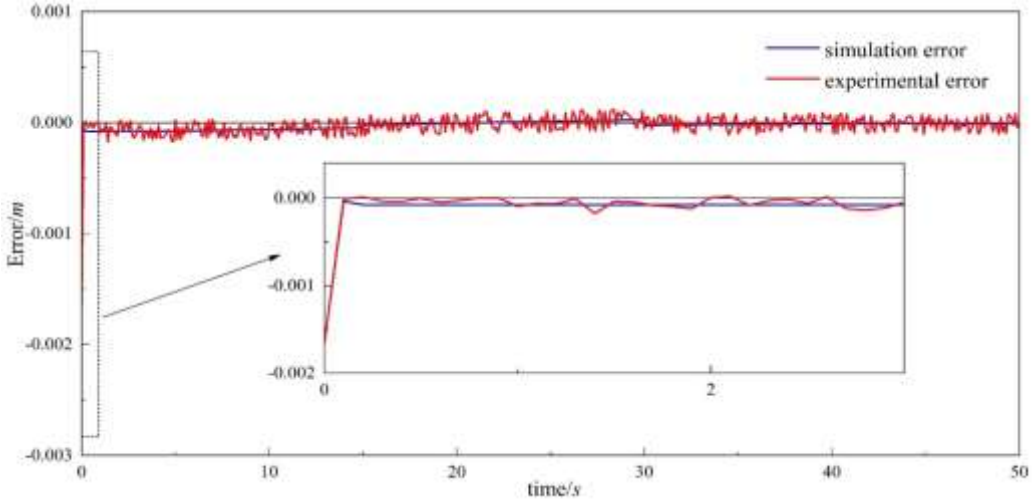

Figure 17 Comparison of Synchronization Errors between Experimental and Simulation Results for Hydraulic Cylinder 3

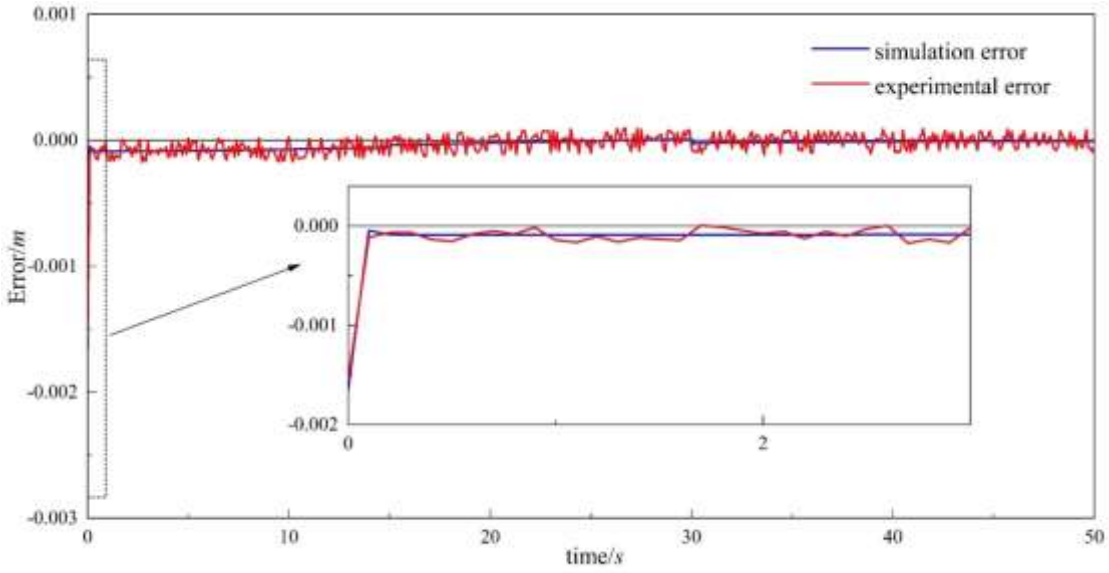

Figure 18 Comparison of Synchronization Errors between Experimental and Simulation Results for Hydraulic Cylinder 4

Table 2 Table of Experimental and simulation displacement error data

Operating Condition	Validation Type	Max Position Error
Test Condition	Simulation（Cylinder 1）	1.60 mm
	Experiment（Cylinder 1）	1.61 mm
	Simulation（Cylinder 2）	1.65 mm
	Experiment（Cylinder 2）	1.66 mm
	Simulation（Cylinder 3）	1.55 mm
	Experiment（Cylinder 3）	1.66 mm
	Simulation（Cylinder 4）	1.56 mm
	Experiment（Cylinder 4）	1.65 mm

6. Conclusion

This study addresses the multi-cylinder synchronous control problem under time-varying and high-pressure constant load conditions via sliding mode robust control of a multi-cylinder hydraulic system. The coupled forces within the subsea drilling rig frame during multi-cylinder synchronous motion are analyzed. Based on a single-cylinder hydraulic model, an integrated multi-cylinder mathematical model is developed. An improved coupling deviation is introduced on the basis of deviation and cross-coupling synchronization errors, and an adaptive algorithm is incorporated to update system parameters. A sliding mode robust synchronous controller for four cylinders is designed. Simulations demonstrate that the proposed adaptive sliding mode robust control algorithm, which incorporates the improved coupling deviation and adaptive mechanism, exhibits high stability, strong robustness, and high synchronization control accuracy under both lifting and lowering operating conditions.

Acknowledge

This work was supported by the National Key R&D Program of China under (Grant No. 2021YFB3401400)

Reference

1. Li J, Ye J, Qin X, et al. The first offshore natural gas hydrate production test in South

China Sea[J]. China geology, 2018, 1(1): 5-16. https://doi.org/10.31035/cg2018003
2. Aly A A. Model reference PID control of an electro-hydraulic drive[J]. International Journal of Intelligent Systems and Applications (IJISA), 2012, 11: 24-32. https://doi.org/10.5815/ijisa.2012.11.03
3. Zuo X, Liu J W, Wang X, et al. Adaptive PID and model reference adaptive control switch controller for nonlinear hydraulic actuator[J]. Mathematical Problems in Engineering, 2017,1-15. https://doi.org/10.1155/2017/6970146
4. Isidori A, Byrnes C I. Output regulation of nonlinear systems[J]. IEEE Transactions on Automatic Control, 1990, 35(2): 131-140. https://doi.org/10.1109/9.45168
5. Guo L C, Liu J W. Improved backstepping control for stochastic high-order nonlinear time delay system with a constructive mechanical system[J]. Transactions of the Institute of Measurement and Control, 2018, 40(15):4115-4124. https://doi.org/10.1177/014 2331217741955
6. Mayne D. Nonlinear and adaptive control design[J]. IEEE Transactions on Automatic Control, 2002,41(12):1849. https://doi.org/10.1109/TAC.1996.545757
7. Kim H M, Park S H, Song J H, et al. Robust position control of electro-hydraulic actuator systems using the adaptive back-stepping control scheme[J]. Proceedings of the Institution of Mechanical Engineers, 2010, 224(6):737-746. https://doi.org/10.1243/09596 518JSCE980
8. Won D, Kim W, Tomizuka M. Nonlinear control with high-gain extended state observer for position tracking of electro-hydraulic systems [J]. IEEE/ASME Transactions on Mechatronics, 2020, 25(6): 2610-2621. https://doi.org/10.1109/TMECH.2020.2985619
9. Du Z F, Chen X Y, Zhang Q W, et al. An extended state observer-based sliding mode control method for hydraulic servo system of marine stabilized platforms[J]. Ocean Engineering, 2023, 279: 114386. https://doi.org/10.1016/j.oceaneng.2023.114386
10. Xu Z Q, Wang Z Y, Shen Z X, et al. Nonlinear differential and integral sliding mode control for wave compensation system of ship-borne manipulator[J]. Measurement and Control, 2021, 54(5-6): 711-723. https://doi.org/10.1177/0020294020944956
11. Qiang H Y, Xie S, Xu Z Q, et al. An enhanced sliding mode control method for wave compensation system of ship-mounted cranes with roll motions and parametric uncertainties[J]. Journal of Marine Science and Technology, 2020, 28(6): 507-517. https://doi.org/10.6119/JMST.202012_28(6).0006
12. Dang X, Zhao X, Dang C, et al. Incomplete differentiation-based improved adaptive backstepping integral sliding mode control for position control of hydraulic system[J]. ISA Transactions, 2020, 109. https://doi.org/10.1016/j.isatra.2020.10.027
13. Yang M X, Zhang Q, Lu X L, et al. Adaptive sliding mode control of a nonlinear electro-hydraulic servo system for position tracking [J]. Mechanics, 2019, 25(4): 283-290. https://doi.org/10.5755/j01.mech.25.4.22822
14. Tang Z Y, Pei P, Wen M, et al. Two novel reaching laws and their use in sliding mode control of EHA[C]. 2015 IEEE International Conference on Information and Automation, IEEE, 2015: 1441-1446. https://doi.org/10.1109/ICInfA.2015.7279513
15. Tran D T, Do T C, Ahn K K. Extended high gain observer-based sliding mode control for an electro-hydraulic system with a variant payload[J]. International Journal of Precision Engineering and Manufacturing, 2019, 20(12):2089-2100. https://doi.org/10.1007/s12 541-019-00256-0
16. Sun C G, Dong X X, Wang M J, et al. Sliding mode control of Electro-Hydraulic position

servo system based on adaptive reaching law[J]. Applied Sciences, 2022, 12(14): 6897. https://doi.org/10.3390/app12146897

17. Huang W, Zhao J, Yu G K, et al. Intelligent vibration control for semiactive suspension systems without prior knowledge of dynamical nonlinear damper behaviors based on improved extreme learning machine[J]. Ieee-Asme Transactions On Mechatronics, 2020,26(4):2071-2079. https://doi.org/10.1109/TMECH.2020.3031840
18. Shi J W, Li X W, Zhang J W. Feedback linearization and sliding mode control for active hydropneumatic suspension of a special-purpose vehicle[J]. Proceedings of the Institution of Mechanical Engineers, Part D: Journal of Automobile Engineering, 2010, 224(1): 41-53. https://doi.org/10.1243/09544070JAUTO1111
19. Lorenz R D, Schmidt P B. Synchronized motion control for process automation[C]. //Conference Record of the IEEE Industry Applications Society Annual Meeting, IEEE, 1989:1693-1698. https://doi.org/10.1109/IAS.1989.96869
20. Zhang L, Li S L, Liu G F. The synchronous control study of once forming leafspring rolling mill[C]. //Advanced Materials Research. Trans Tech Publications Ltd, 2012, 383:1867-1872.https://doi.org/10.4028/www.scientific.net/AMR.383-390.1867
21. Zhang L, Li Y. Synchronous control of double hydraulic cylinders of scissors aerial work platform based on fuzzy PID[C]. //2020 5th International Conference on Electromechanical Control Technology and Transportation (ICECTT). IEEE, 2020: 349-354. https://doi.org/10.1109/ICECTT50890.2020.00084
22. Yoram, Koren. Cross-coupled biaxial computer control for manufacturing systems [J]. Journal of Dynamic Systems, Measurement, and Control, 1980, 102(4): 265-272. https://doi.org/10.1115/1.3149612
23. Yang C, Huang Q, Han J. Decoupling control for spatial six-degree-of-freedom electro-hydraulic parallel robot[J]. Robotics and Computer Integrated Manufacturing, 2011, 28(1):14-23. https://doi.org/10.1016/j.rcim.2011 .06.002